Changes in the Isotopic Signature of Atmospheric Nitrous Oxide and Its Global Average Source During the Last Three Millennia

Prokopiou, M.; Sapart, C. J.; Rosen, J.; Sperlich, P.; Blunier, T.; Brook, E.; van de Wal, R. S. W.; Rockmann, T.

Published in:
Journal of Geophysical Research: Atmospheres

DOI:
10.1029/2018JD029008

Publication date:
2018

Document version
Publisher's PDF, also known as Version of record

Journal of Geophysical Research: Atmospheres

RESEARCH ARTICLE
10.1029/2018JD029008

Key Points:
- The isotopic composition of nitrous oxide in the preindustrial period was determined with high precision
- The isotopic composition of nitrous oxide changed during the transition to the industrial period
- The temporal evolution of $\delta^{15}N^{av}$ is different from that of $\delta^{18}O$ implying a decoupling of sources over the industrial period

Changes in the Isotopic Signature of Atmospheric Nitrous Oxide and Its Global Average Source During the Last Three Millennia

M. Prokopiou[1], C. J. Sapart[1,2], J. Rosen[3], P. Sperlich[4,5], T. Blunier[5], E. Brook[3], R. S. W. van de Wal[1], and T. Röckmann[1]

[1]Institute for Marine and Atmospheric research Utrecht, Utrecht University, Utrecht, Netherlands, [2]Laboratoire de Glaciologie, Université Libre de Bruxelles, Brussels, Belgium, [3]College of Earth, Ocean, and Atmospheric Sciences, Oregon State University, Corvallis, OR, USA, [4]National Institute of Water and Atmospheric Research, Wellington, New Zealand, [5]Centre for Ice and Climate, Niels Bohr Institute, University of Copenhagen, Copenhagen, Denmark

Abstract Nitrous oxide (N_2O) is a strong greenhouse gas whose mole fraction in the atmosphere has increased over the industrial period. We present a new set of isotope measurements of N_2O in air extracted from ice cores covering the last 3,000 years. For the preindustrial (PI) atmosphere, we find an average N_2O mole fraction of (267 ± 1) nmol/mol and average tropospheric N_2O isotopic values of $\delta^{15}N^{av}_{PI}$ = (9.5 ± 0.1)‰, $\delta^{18}O_{PI}$ = (47.1 ± 0.2)‰, $\delta^{15}N^{\alpha}_{PI}$ = (17.8 ± 0.4)‰, and $\delta^{15}N^{\beta}_{PI}$ = (1.2 ± 0.4)‰. From PI to modern times all isotope signatures decreased with a total change of $\delta^{15}N^{av}$ = (−2.7 ± 0.2)‰, $\delta^{18}O$ = (−2.5 ± 0.4)‰, $\delta^{15}N^{\alpha}$ = (−2.0 ± 0.7)‰, and $\delta^{15}N^{\beta}$ (−3.5 ± 0.7)‰. Interestingly, the temporal evolution is not the same for $\delta^{15}N^{av}$ and $\delta^{18}O$. $\delta^{18}O$ trends are relatively larger during the early part, and $\delta^{15}N^{av}$ trends are larger during the late part of the industrial period, implying a decoupling of sources over the industrial period. Using a mass balance model, we determined the isotopic composition of the total average N_2O source. Assuming that the total present source is the sum of a constant natural source and an increasing anthropogenic source, this anthropogenic source has an isotopic signature of $\delta^{15}N^{av}_{source,anthrop}$ = (−15.0 ± 2.6)‰, $\delta^{18}O_{source,anthrop}$ = (30.0 ± 2.6)‰, $\delta^{15}N^{\alpha}_{source,anthrop}$ = (−4.5 ± 1.7)‰, and $\delta^{15}N^{\beta}_{source,anthrop}$ = (−24.0 ± 8.4)‰. The ^{15}N site preference of the source has increased since PI times, which is indicative of a relative shift from denitrification to nitrification sources, consistent with agricultural emissions playing a major role in the N_2O increase.

Correspondence to:
M. Prokopiou,
markella.prokopiou@gmail.com

Citation:
Prokopiou, M., Sapart, C. J., Rosen, J., Sperlich, P., Blunier, T., Brook, E., van de Wal, R. S. W., & Röckmann, T. (2018). Changes in the isotopic signature of atmospheric nitrous oxide and its global average source during the last three millennia. *Journal of Geophysical Research: Atmospheres*, *123*, 10,757–10,773. https://doi.org/10.1029/2018JD029008

Received 14 MAY 2018
Accepted 26 AUG 2018
Accepted article online 31 AUG 2018
Published online 24 SEP 2018

1. Introduction

Nitrous oxide (N_2O) is an important long-lived greenhouse gas that contributes significantly to the increased radiative forcing of the climate system (Forster et al., 2007; Stocker et al., 2013). Ice core and firn data of N_2O mole fraction have been reported extending back 800,000 years before present and show pronounced glacial-interglacial variability with values as low as 200 nmol/mol during glacial periods and up to 280 nmol/mol during interglacial periods (Bernard et al., 2006; Flückiger et al., 2002; Ishijima et al., 2007; MacFarling Meure et al., 2006; Röckmann, Kaiser, & Brenninkmeijer, 2003; Schilt, Baumgartner, Blunier, et al., 2010; Schilt, Baumgartner, Schwander, et al., 2010; Sowers et al., 2003, 2002). Since 1750 the mole fraction of N_2O in the atmosphere has steadily increased and is currently about (330 ± 1) nmol/mol, a value that is unprecedented in the ice core record.

Global N_2O production is largely attributed to microbial sources. Bacteria and archaea produce N_2O through nitrification and denitrification. Nitrification is the main source of N_2O under aerobic conditions, while denitrification dominates under anoxic conditions (Denk et al., 2017; Ostrom & Ostrom, 2011; Toyoda et al., 2015). The main sink of N_2O is destruction in the stratosphere, through UV photolysis (~90%) and reactions with excited oxygen atoms (~10%; Minschwaner et al., 1993).

Microbial sources can be both natural and anthropogenic. Natural sources represent processes in uncultivated soils, oceans, and other aquatic systems (EPA, 2010). Anthropogenic microbial emissions are associated with agricultural emissions and are strongly affected by the use of synthetic fertilizers (Kroeze et al., 1999). Other anthropogenic sources are fossil fuel combustion, especially from automobiles, industrial processes (nylon production), and biomass burning (Syakila & Kroeze, 2011).

The N_2O budget is difficult to constrain mainly due to the long N_2O residence time in the atmosphere (123^{+29}_{-19} year, SPARC, 2013), resulting in small temporal and spatial gradients, and because N_2O production varies strongly spatially and temporally, which complicates scaling up from local measurements.

Global estimates of N_2O emissions are based on bottom-up (summing individual source estimates) and top-down (using atmospheric measurements to constrain sources) approaches, which mainly rely on atmospheric mole fraction measurements. The preindustrial (henceforth PI) N_2O flux derived by both methods is ≈(11.0 ± 1.7) Tg N/year (Stocker et al., 2013). Current estimates suggest that during PI times 63% of the natural sources originated from microbial production in soils and 37% from oceans (Stocker et al., 2013). Currently, the total annual flux of N_2O is estimated to be 16 to 20 Tg N/year (Denman et al., 2007; Syakila & Kroeze, 2011; Thompson et al., 2014). Bottom-up model calculations suggest that of the anthropogenic emissions 1 Tg N/year is due to nitrogen deposition to oceans from anthropogenic processes (Duce et al., 2008), 4–6 Tg N/year is due to agricultural emissions, 1.2–1.5 Tg N/year originates from the energy and industry sector, and 0.7 Tg N/year is from biomass burning (Syakila & Kroeze, 2011).

Although the understanding of N_2O production processes has strongly improved, the contributions from the individual source categories are not well constrained. For example, nitrification appears to dominate oceanic N_2O emissions, but denitrification hot spots have been identified in low oxygen availability areas, coastal sediments, and estuaries (Bange et al., 2005; Ji et al., 2015).

Culture studies have revealed more information on the specific organisms and environments responsible for marine N_2O production. Ammonia oxidizing bacteria were long believed to be the main oceanic source, but recently ammonia oxidizing archaea were identified as a key N_2O source (Löscher et al., 2012; Santoro et al., 2011). In terrestrial ecosystems, denitrification appears to control N_2O emissions, while agricultural soils show enhancement in both nitrification and denitrification. Pérez et al. (2001) suggested that fertilizer applications favor nitrification, but it has proven difficult to quantify this on a global scale.

A way to further constrain the N_2O budget is to measure its isotopic composition. Studies have determined the isotopic composition of atmospheric N_2O from atmospheric monitoring locations and in polar firn (Bernard et al., 2006; Ishijima et al., 2007; Park et al., 2012; Prokopiou et al., 2017; Röckmann & Levin, 2005; Röckmann, Kaiser, & Brenninkmeijer, 2003; Sowers et al., 2002; Toyoda et al., 2013) in order to provide additional information on temporal changes of N_2O emissions. Firn air records, though, only cover up to 100 years of recent atmospheric history and most of them only several decades. Air bubbles trapped in polar ice cores provide an air archive that extends much further back in time. The ^{18}O and bulk ^{15}N content of N_2O are reported in delta notation as $\delta^{18}O$ and $\delta^{15}N^{av}$, respectively, and $\delta^{15}N^{av}$ is the average of the ^{15}N content of the central (α) and terminal (β) nitrogen position, $\delta^{15}N^{av} = 0.5 \times (\delta^{15}N^{\alpha} + \delta\ ^{15}N^{\beta})$; see section 2.3 for definition of the delta value.

Only a small number of studies focused on the isotopic composition of N_2O from ice core samples. Sowers et al. (2002) combined ice core data from Greenland Ice Sheet Project (GISP) II, Greenland, with firn air data to reconstruct the $\delta^{15}N^{av}$ and $\delta^{18}O$ isotopic history of N_2O between 1785 and 1990 (Common Era [CE]). They suggested that the $\delta^{15}N^{av}$ and $\delta^{18}O$ trends possibly varied at different rates during different stages of the industrial period. Such a potential decoupling of $\delta^{15}N^{av}$ and $\delta^{18}O$ would imply that the increase of N_2O since PI times is not due to one single *anthropogenic* source with a certain isotopic composition but consists of several source components. Alternatively, the isotopic composition of the source could have changed over time. On the other hand, Bernard et al. (2006) reported much more consistent $\delta^{15}N^{av}$ and $\delta^{18}O$ trends between ice core and firn air studies using samples from North Greenland Ice Core Project, Greenland, and Berkner Island, Antarctica. Both studies analyzed a limited amount of ice core samples, and considering that the analytical errors for ice core measurements are quite large, the question of a possible decoupling of $\delta^{15}N^{av}$ and $\delta^{18}O$ remained unresolved.

In an attempt to reconstruct variations of natural sources of N_2O in the past, Schilt et al. (2014) reported the $\delta^{15}N^{av}$ and $\delta^{18}O$ isotopic composition of N_2O between 16 and 10 ka before present from Taylor Glacier in Antarctica and concluded that both terrestrial and marine sources contributed roughly equally to the observed increase of N_2O from the glacial to the interglacial periods. Terrestrial emissions dominate

variability on centennial to millenial time scales probably influenced by temperature and precipitation patterns over land surfaces.

In this study we present measurements of the isotopic composition of N_2O in the PI atmosphere from Greenland ice core samples covering the last 3,000 years. The data allow us to tightly constrain the isotopic composition of N_2O in the PI atmosphere, investigate possible variations in the N_2O budget in the PI period, and constrain the decoupling of $\delta^{15}N^{av}$ and $\delta^{18}O$ over the industrial period much more precisely than previous studies.

2. Methodology

2.1. Ice Core Collection

Of the new 39 ice core samples that were analyzed in this study, 30 were collected in 2008 as part of the North Eemian Ice Drilling Programme (NEEM) in Greenland. The NEEM drilling site (77.45°N, 51.06°W, 2,450 m elevation) currently has a mean annual temperature of −29 °C and a surface accumulation rate of 22 cm ice equivalent per year (NEEM community paper). An additional nine samples from the Eurocore Greenland project (drilled in 1989) were analyzed (EUROCORE_NM). The site is located at 72.56°N, 38.45°W, 3,240 m altitude and has a mean annual temperature of −32 °C and surface accumulation rate of 21 cm water equivalent per year. For the scientific interpretation we combine these 39 new samples with results from 13 ice core samples collected from the Siple Dome A ice core that were analyzed previously on the same analytical system (Rosen, 2014; Taylor et al., 2004). This core was drilled in 1999 in coastal West Antarctica (81.65°N, 148.81°W) at an elevation of 621 m above sea level.

The age of the NEEM ice was calculated using a gas age chronology, following the GICC05 time scale, which is based on many overlapping data series from three different cores, utilizing the best available data for each time period. Overlap between the different sections ensures consistency between the different parts of the time scale and yield a typical dating error of 0.5% (Vinther et al., 2006). Siple Dome gas age was determined (Rosen, 2014) by matching methane variations with the well-dated methane record from the West Antarctic Ice Sheet Divide ice core Mitchell et al. (2011).

Measurements of the isotopic composition of trace gases from ice cores must be corrected for firn air fractionation (Severinghaus et al., 2001), notably gravitational and diffusive separation of the different isotopocules in the firn column before the air is trapped in the ice. For N_2O isotopocules, the correction is based on the mass difference between the heavier isotopocules and the most abundant $^{14}N^{14}N^{16}O$, thus 1 atomic unit for $\delta^{15}N^{av}$ and 2 for $\delta^{18}O$. The corresponding correction is $<0.5‰$ for the data reported here, and the firn fractionation correction is consistent across the different data sets (Buizert et al., 2013; Severinghaus et al., 2009).

2.2. Isotope Measurement

The isotopic composition of atmospheric N_2O trapped in polar ice was measured by continuous-flow isotope ratio mass spectrometry (IRMS) at the Institute for Marine and Atmospheric research Utrecht, Utrecht University, the Netherlands. The dry extraction measurement technique for ice core samples, which enables simultaneous measurement of the isotopic composition of N_2O and CH_4, has been described in Sapart et al. (2011) and is briefly summarized here.

Ice samples of about 500 g (yielding ≈ (17 ± 1) ng of CH_4 in our extraction system; Sapart et al., 2011) were placed in a perforated ice grating cylinder made of titanium nitride coated stainless steel inside a 6-L-volume stainless steel grating vessel, which was sealed with a copper gasket and fixed in a shaking device mounted in a freezer at −30 °C. The vessel holding the sample was generally evacuated overnight in order to remove all ambient air, reaching a pressure of 10^{-3} mbar. In cases where an analysis of two samples was performed on the same day, the vessel was evacuated until reaching the desired pressure (10^{-3} mbar).

After the system reached the desired pressure (minimum 3 hr of evacuation), the vessel was closed and disconnected from the vacuum line. The ice was grated for ≈25 min during which the angle and the speed of the shaking device were changed stepwise to minimize collisions of ice with the metal and to achieve maximum grating efficiency. The grating vessel was then connected to a glass line consisting of three consecutive U-shaped traps where the air released during grating was extracted. The first trap collected water at −80 °C, the second one trapped CO_2 and N_2O at −196 °C, and the third one was filled with Haysep-D

(mesh 80/100, Alltech GmbH, Germany), a molecular absorbent, cooled to −196 °C, to adsorb CH_4 as well as the major air components (O_2, N_2, and Ar) and other trace gases.

After extraction, all traps were isolated and the contents of traps 2 and 3 (N_2O/CO_2 and CH_4/air, respectively) were flushed with He at ambient temperature to two separated IRMS systems. Before and after each sample was processed, *blank* measurements were performed by filling the traps with pure helium to make sure that no contaminating gas was present before the measurement and no sample gas was left in the traps after the measurement took place.

The N_2O sample passed through a glass tube filled with an Ascarite II® (mesh 8–20, Aldrich chemistry, USA) where the CO_2 was chemically removed. The remaining N_2O and other condensable gases were cryogenically (−196 °C) preconcentrated. After cryofocusing, the N_2O was purified from remaining traces of CO_2 and other contaminants on a capillary gas chromatography column (PoraPLOT Q, 0.32 mm internal diameter [i.d.], 25 m). To avoid interferences from other atmospheric compounds that have longer retention times, the column is separated into a precolumn and an analytical one (Röckmann, Kaiser, Brenninkmeijer, & Brand, 2003). The purified sample was then transferred to the IRMS via an open split interface.

A laboratory reference air bottle with known composition (NAT 332, air collected at Groningen, the Netherlands was measured daily directly before the ice extraction, following the same procedure as the extraction of air from an ice sample, except for the grating. For this purpose, reference air was released into the evacuated stainless steel pot containing an intact ice sample. The air was then extracted and treated as an ice air sample. NAT 332 has a mole fraction of (332.8 ± 0.8) nmol/mol and an isotopic composition of $\delta^{15}N^{av}$ = (6.6 ± 0.7), $\delta^{18}O$ = (45.8 ± 1.3)‰, $\delta^{15}N^{\alpha}$ = (15.6 ± 2.1), and $\delta^{15}N^{\beta}$ = (−2.5 ± 2.1)‰. The stated errors (1σ) indicate the standard deviation for repeated individual measurements (Sapart et al., 2011).

2.3. Data Processing

Isotope deltas (δ) are used to quantify the relative $^{15}N/^{14}N$ and $^{18}O/^{16}O$ ratio difference of N_2O in sample gas air with respect to a reference ratio $R_{standard}$,

$$\delta^{15}N = \frac{R_{sample}}{R_{standard}} - 1 \quad (1)$$

where R represents the $^{15}N/^{14}N$ or $^{18}O/^{16}O$ abundance ratio of a standard or a sample. All δ values pertaining to ^{15}N are reported via air-N_2, and the values for ^{18}O are reported versus Vienna Standard Mean Ocean Water. The $^{15}N/^{14}N$ and $^{18}O/^{16}O$ isotope ratios were derived from *m/z* 45/*m/z* 44 and *m/z* 46/*m/z* 44 ion current ratios according to Kaiser et al. (2003), assuming a constant ^{17}O excess of 0.9‰. For the position-dependent ^{15}N isotopologues the data reduction scheme accounting for isotopic scrambling in the ion source developed by Kaiser and Röckmann (2008) was adopted.

Isotope measurements of another laboratory reference gas (NAT 335, air collected from Centre for Isotope Research, CIO, Groningen, the Netherlands) were performed directly on the IRMS system before and after the sample measurements and injected air volumes were chosen to closely match the expected sample peak areas. The laboratory standard has an N_2O mole fraction of (318 ± 1) nmol/mol and isotope ratios of $\delta^{15}N^{av}$ = (6.4 ± 0.2)‰, $\delta^{18}O$ = (44.9 ± 0.4)‰, $\delta^{15}N^{\alpha}$ = (15.4 ± 1.2)‰, and $\delta^{15}N^{\beta}$ = (−2.7 ± 1.2)‰. The uncertainties of the reference air cylinder involve transfer of the isotope scale over four carefully calibrated reference air cylinders since the N_2O isotope scale of our laboratory was set up by Kaiser et al. (2003). The calibration of the intramolecular distribution has been converted to the scale of Yoshida and Toyoda (2000). These values are used to convert the δ values to the international scales.

2.4. Isotope Budget Calculations

N_2O is almost exclusively emitted from the Earth's surface, with a minor contribution from in situ production in the troposphere (Dentener & Crutzen, 1994; Röckmann et al., 2001), while its removal takes place almost exclusively in the stratosphere (Ishijima et al., 2007; Park et al., 2012; Röckmann, Kaiser, & Brenninkmeijer, 2003; Rahn and Wahlen, 2000; Sowers et al., 2002). As the isotope effect in the stratospheric removal is well constrained by in situ measurements (e.g. Kaiser et al., 2006), the isotopic composition of the source can be calculated in a simple mass balance model from the observed trend in the isotopic composition of the

Table 1
Input Values to Establish the Average Source Isotopic Signature During PI and Modern Periods

	Model Parameters	
	PI >1750 CE	Modern 1989–2008 CE
Burden (Tg N)[a]	1,096 ± 18	1,313 ± 18
$\frac{\partial\delta_{Trop}}{\partial t}$ (‰/year)[b]	0	$\delta^{15}N^{av} = -0.036 \pm 0.004$ $\delta^{18}O = -0.014 \pm 0.001$ $\delta^{15}N^{\alpha} = -0.024 \pm 0.002$ $\delta^{15}N^{\beta} = -0.040 \pm 0.004$
Σsources (Tg N/year)[c]	10.6 ± 2.6	15.5 ± 3.9
δ_{Trop} (‰)[d]	$\delta^{15}N^{av} = 9.5 \pm 0.1$ $\delta^{18}O = 47.1 \pm 0.2$ $\delta^{15}N^{\alpha} = 17.8 \pm 0.4$ $\delta^{15}N^{\beta} = 1.2 \pm 0.4$	$\delta^{15}N^{av} = 6.8 \pm 0.2$ $\delta^{18}O = 44.6 \pm 0.1$ $\delta^{15}N^{\alpha} = 15.8 \pm 0.1$ $\delta^{15}N^{\beta} = -2.3 \pm 0.2$
L (Tg N/year)[c]	10.6 ± 2.6	12.7 ± 3.2
ε (‰)[e]	$\varepsilon^{15}N^{av} = -16.2 \pm 0.5$ $\varepsilon^{18}O = -13.4 \pm 0.7$ $\varepsilon^{15}N^{\alpha} = -23.0 \pm 1.4$ $\varepsilon^{15}N^{\beta} = -8.7 \pm 1.1$	

Note. Uncertainty is expressed as one standard deviation. PI = preindustrial; LI = late industrial; NEEM = North Eemian Ice Drilling Programme; EUROCORE_NM = Eurocore Greenland project.
[a]Burden was calculated using the average mole fraction values for each period (PI, LI), and the uncertainty was assumed to be 25%. [b]$\frac{\partial\delta_{Trop}}{\partial t}$ was calculated using the average total change from transitioning from one period to another and dividing it by the number of total years. For PI times it was assumed that there was a balance in the troposphere-stratosphere exchange and this number was null. For modern times the rates were calculated using the tropospheric values from Prokopiou et al. (2017) firn air reconstruction over the last 20 years. [c]The values were calculated based on the equations from Prokopiou et al. (2017) were the PI atmosphere was assumed to be in balance and in the EI and LI periods the loss strength was assumed to be proportional to the tropospheric concentration; that is, the rate coefficient for the loss was assumed constant during the investigated period. We assumed 25% uncertainty. [d]The tropospheric values used as input are the average isotope tropospheric values as measured from air trapped in ice cores for the purpose of this study. The PI values are the averaged values from 30 NEEM, 2 EUROCORE_NM, and 9 Siple Dome ice core samples. The modern values were calculated using the average tropospheric values from Prokopiou et al. (2017) firn air reconstruction over the last 20 years. [e]The apparent fractionation values are averaged values from Table 2 in Kaiser et al. (2006), and the uncertainty is the average of all individual errors reported there.

tropospheric reservoir. Several equivalent box models have been used in the past, and we use here the representation of Snider et al. (2015) to calculate the isotopic signature of the total N_2O source:

$$N_T \frac{\partial\delta_T}{\partial t} = P(\delta_P - \delta_T) - L(\delta_L - \delta_T) \quad (2)$$

where N_T is the tropospheric burden of N_2O; P and L are the total source and loss strengths, respectively; δ_L, δ_P, and δ_T are the δ values associated with the loss, production, and the tropospheric value, respectively; δ_P is the target quantity we want to solve for; and $\frac{\partial\delta_T}{\partial t}$ is the deseasonalized linear trend in the isotopic composition of the tropospheric N_2O reservoir over the respective period.

Following Park et al. (2012), the loss term can be approximated as

$$L(\delta_L - \delta_T) \approx L\varepsilon_{app} \quad (3)$$

where ε_{app} is the apparent fractionation associated with the N_2O destruction process in the stratosphere, for which we used the averaged measured values from stratospheric observations using air samples collected on high-altitude balloon flights (Kaiser et al., 2006; average of values in Table 2).

Then, equation (2) can be solved for the isotopic signature of the global average N_2O source.

$$\delta_P = \frac{N_T \frac{\partial\delta_T}{\partial t} + L\varepsilon_{app} + P\delta_T}{P} \quad (4)$$

We solve equation (4) for the PI and present atmosphere. For the PI atmosphere we assume a steady state in the isotopic composition, thus, $\frac{\partial\delta_T}{\partial t} = 0$; in agreement with our data (see Tables 1, 2 and section 4.1) and for the present period we use linear trend estimates derived from the new ice core measurements and the firn reconstruction from Prokopiou et al. (2017). The values used as input for our calculations are given in Table 1.

Having calculated the total global average source signatures, we split the source for the present atmosphere into a *natural* contribution and a time-dependent anthropogenic contribution using a simple mass balance calculation. Here the natural source is the same as the source calculated for the PI atmosphere, and it is assumed constant. The anthropogenic source is assumed to vary in strength but has a constant isotope signature. We acknowledge that these are strong assumptions, which may not be fully adequate. For example, natural emissions may be different during the present climate state compared to 1750, and the time-dependent anthropogenic source may not be isotopically constant over time. We discuss some of these potential biases and possible additional variability in section 4.

3. Results

Figure 1a shows the temporal evolution of the N_2O mole fraction and isotopic composition as derived from our NEEM, EUROCORE_NM, and Siple Dome ice core measurements, along with previously published data. The year 1750 CE marks the start of the industrial revolution, and in the following we refer to the period before 1750 as PI. We furthermore split the industrial period into two parts, the *early industrial* (EI) period (1750–1940) that is mainly represented by ice core samples, which extend to 1940, and a *late industrial* (LI) period (1940–2008) that is represented by firn air measurements (Prokopiou et al., 2017, see below). We note that this split is largely operational in nature (firn and ice core samples), but it also separates a period of relatively slow increase in N_2O before 1940 from a period with faster increase after 1940 (where the transition is

Table 2
Average Source Isotopic Composition in the PI and Modern Periods as Calculated Using a Mass Balance Model and Compared With Studies From Snider et al. (2015), Park et al. (2012), Ishijima et al. (2007), Röckmann, Kaiser, and Brenninkmeijer (2003), and Sowers et al. (2002)

	$\delta_{source,\ PI}$		$\delta_{source,\ mod}$		$\delta_{source,\ anthrop}$					
	This study	Park et al. (2012)	This study	Snider et al. (2015)	This study	Prokopiou et al. (2017)	Park et al. (2012)	Ishijima et al. (2007)	Röckmann, Kaiser, and Brenninkmeijer (2003)	Sowers et al. (2002)
$\delta^{15}N^{av}$ (‰)	−6.8 ± 0.1	−5.3 ± 0.2	−9.5 ± 0.9	−8.3 ± 4.0	−15.0 ± 2.6	−18.2 ± 2.6	−15.6 ± 1.2	−6 to −19	−11.5	−7 to−13
$\delta^{18}O$ (‰)	33.7 ± 0.2	32.0 ± 0.2	32.5 ± 0.8	31.7 ± 13.9	30.0 ± 2.6	27.2 ± 2.6	32.0 ± 1.3	20 to 40	31.3	17 to 26
$\delta^{15}N^{\alpha}$ (‰)	−5.2 ± 0.4	−3.3 ± 1.0	−5.0 ± 1.4	NA	−4.5 ± 1.7	−8.1 ± 1.7	−7.6 ± 6.2	NA	−5.6	NA
$\delta^{15}N^{\beta}$ (‰)	−7.5 ± 0.4	−7.5 ± 1.1	−12.8 ± 2.2	NA	−24.0 ± 8.4	−26.1 ± 8.4	−20.5 ± 7.1	NA	−17.8	NA
SP = $\delta^{15}N^{\alpha} - \delta^{15}N^{\beta}$	2.3 ± 0.7	4.2 ± 1.5	7.8 ± 2.6	NA	19.5 ± 8.6	18.0 ± 8.6	12.9 ± 9.4	NA	12.2	NA

Note. PI = preindustrial; SP = site preference; NA = Not Available.

of course gradual). Average values over the last 20 years (1989–2008) of the reconstruction of Prokopiou et al. (2017) will be referred to as *modern* values.

During the PI period, the N_2O mole fraction was (267 ± 2) nmol/mol (uncertainty given is standard error of the mean) and showed only minor variability, between 262 and 270 nmol/mol. During the EI period the N_2O mole fraction gradually increased, reaching (285 ± 2) nmol/mol in 1940 (CE). We show all mole fraction data from both hemispheres combined because the interhemispheric difference is very small for N_2O and only detectable in modern high precision and high time resolution measurement series (Hirsch et al., 2006).

Figures 1b–1e show the new ice core record of $\delta^{15}N^{av}$, $\delta^{18}O$, $\delta^{15}N^{\alpha}$, and $\delta^{15}N^{\beta}$ from NEEM, EUROCORE_NM, and Siple Dome along with data from GISP II (Sowers et al., 2002) and North Greenland Ice Core Project and Berkner Island (Bernard et al., 2006). Ice core samples from Siple Dome and Bernard et al. (2006) were measured with the same analytical system as the NEEM samples, whereas the samples from Sowers et al. (2002) were measured in a different laboratory. Unfortunately, no direct intercomparison between the two laboratories has been made; thus, there may be some scale differences. However, Figure 1 shows that such differences are likely not very large and they will not affect the conclusions below. Similar to the mole fraction it is not possible to detect interhemispheric differences in isotopic composition with the existing data sets over the PI period.

The average isotopic composition of N_2O in the PI period is $\delta^{15}N^{av}_{PI}$ = (9.5 ± 0.1)‰, $\delta^{18}O_{PI}$ = (47.1 ± 0.2)‰, $\delta^{15}N^{\alpha}_{PI}$ = (17.8 ± 0.4)‰, and $\delta^{15}N^{\beta}_{PI}$ = (1.2 ± 0.4)‰ (Tables 1 and 2; stated uncertainties are standard error of the mean). The ^{15}N isotopomer signatures, $\delta^{15}N^{\alpha}$ and $\delta^{15}N^{\beta}$, have larger uncertainties and show larger scatter compared to $\delta^{15}N^{av}$ and $\delta^{18}O$, which is due to the lower precision of the isotopomer measurements.

Parallel to the increase in the mole fraction during the EI period from 1750 to 1940, $\delta^{15}N^{av}$ and $\delta^{18}O$ gradually decrease. The averages over the EI period are $\delta^{15}N^{av}_{EI}$ = (8.9 ± 0.3)‰ and $\delta^{18}O_{EI}$ = (45.8 ± 0.5)‰. $\delta^{15}N^{\alpha}_{EI}$ shows a small nonsignificant increase to (18.3 ± 0.6)‰ and $\delta^{15}N^{\beta}_{EI}$ decreases to (0.6 ± 0.5)‰. We realize that taking averages over periods with clear temporal trends like the EI period likely introduce an additional error that is hard to quantify. The averages reported here are simple arithmetical averages (not mole fraction weighted) and may be biased by uneven sampling, so they should be interpreted with caution.

Figure 2a shows the isotopic composition of N_2O of the PI and modern troposphere, the PI and modern global source signature, according to the mass balance model of equation (4), and the anthropogenic source signature. The total average source isotopic signatures are $\delta^{15}N^{av}_{source,LI}$ = (−9.5 ± 0.9)‰ and $\delta^{18}O_{source,LI}$ = (32.5 ± 0.8)‰, respectively, while the corresponding PI values are $\delta^{15}N^{av}_{source,PI}$ = (−6.8 ± 0.1)‰ and $\delta^{18}O_{source,PI}$ = (33.7 ± 0.2)‰, respectively. These PI values are in agreement within uncertainties with previous studies (see Table 2). The results of the modern total average source signature agree with a recent bottom-up study from Snider et al. (2015) who estimated the average values of $\delta^{15}N^{av}$ and $\delta^{18}O$ to be (−8.4 ± 4.0)‰ and (31.7 ± 13.9)‰, respectively.

Assuming that the natural (=PI) source remained unchanged in strength and isotopic signature yields an average isotopic signature of the total anthropogenic source of $\delta^{15}N^{av}_{source,anthrop}$ = (−15.0 ± 2.6)‰ and

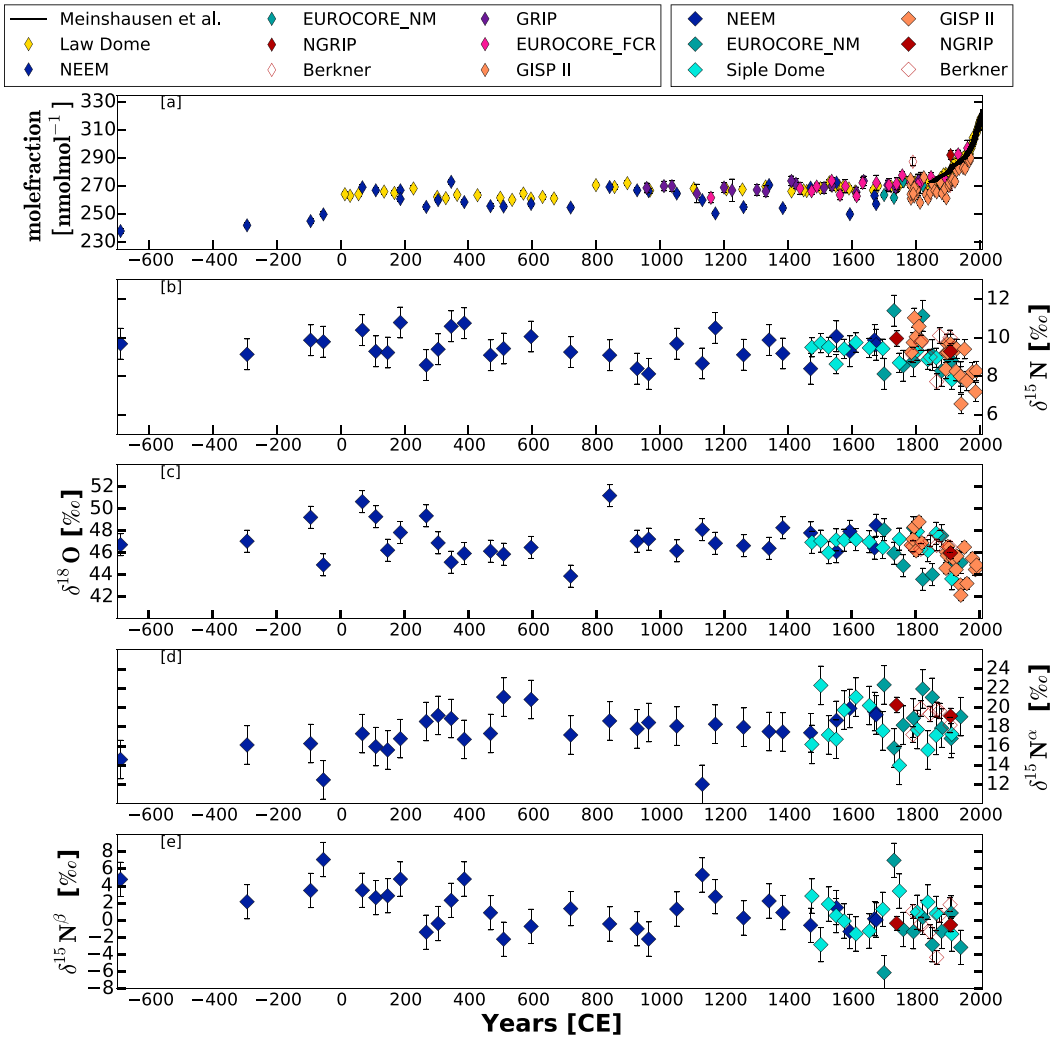

Figure 1. NEEM N_2O ice core data results covering the last three millennia (CE). (a) N_2O mole fraction from NEEM (blue diamonds), EUROCORE_NM (green diamonds), Law Dome (yellow diamonds; MacFarling Meure et al., 2006), Berkner Island (white diamonds; Bernard et al., 2006), and a combination of ice and firn studies (black line; Meinshausen et al., 2017), GISP II (orange diamonds; Sowers et al., 2002), GRIP (purple diamonds), EUROCORE_FCR (pink diamonds; Flückiger et al., 2002), and NGRIP (red diamonds; Bernard et al., 2006). (b)–(e) $\delta^{15}N^{av}$, $\delta^{18}O$, $\delta^{15}N^{\alpha}$, and $\delta^{15}N^{\beta}$ in per mille. The color coding is the same as for mole fraction; cyan diamonds show data from Siple Dome (Rosen, 2014). NEEM = North Eemian Ice Drilling Programme; EUROCORE_NM = Eurocore Greenland project; GISP = Greenland Ice Sheet Project; NGRIP = North Greenland Ice Core Project.

$\delta^{18}O_{source,anthrop}$ = (30.0 ± 2.6)‰. As has been shown in previous studies, the present N_2O source is isotopically lighter than the natural source, and the anthropogenic component is depleted in ^{15}N and ^{18}O relative to the natural source. The relative depletion is even larger for ^{15}N than for ^{18}O.

Figure 2b shows a similar plot for $\delta^{15}N^{\alpha}$ versus $\delta^{15}N^{\beta}$. The total average source isotopic signatures of $\delta^{15}N^{\alpha}$ and $\delta^{15}N^{\beta}$ for the modern period are $\delta^{15}N^{\alpha}_{source,mod}$ = (−5.0 ± 1.4)‰ and $\delta^{15}N^{\beta}_{source,mod}$ = (−12.8 ± 2.2)‰, respectively, while the corresponding PI values are $\delta^{15}N^{\alpha}_{source,PI}$ = (−5.2 ± 0.4)‰ and $\delta^{15}N^{\beta}_{source,PI}$ = (−7.5 ± 0.4)‰, respectively. The calculated total average anthropogenic source signatures are $\delta^{15}N^{\alpha}_{source,anthrop}$ = (−4.5 ± 1.7)‰ and $\delta^{15}N^{\beta}_{source,anthrop}$ = (−24.0 ± 8.4)‰.

4. Discussion

4.1. The Isotopic Composition of N_2O in the PI Atmosphere

Our experimental results are generally consistent with two earlier studies that have analyzed the isotopic composition of N_2O in PI and EI ice (Bernard et al., 2006; Sowers et al., 2002; Table 3). However, the data

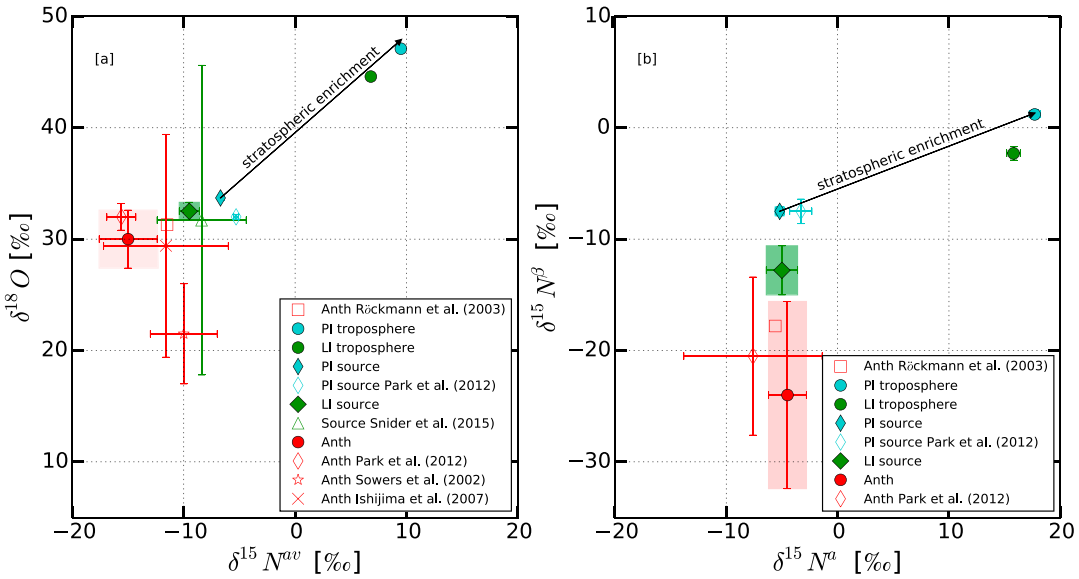

Figure 2. (a) $\delta^{15}N^{av}$ and $\delta^{18}O$ of the tropospheric N_2O reservoir for PI (cyan circle) and modern (green circle) periods, and total average source for the same period with uncertainty bars (same coloring in diamonds). The red circle indicates the average anthropogenic source signature as calculated from this study. Results are compared with previous studies as stated in the legend, and the shaded areas in corresponding colors show the estimated range of the sources. The arrows represent the isotopic enrichment associated with the stratospheric loss. (b) $\delta^{15}N^{\alpha}$ and $\delta^{15}N^{\beta}$ tropospheric N_2O reservoir for PI (cyan circle) and modern (green circle) periods, and total average source for the same period with uncertainty bars (in diamonds). The red circle indicates the average anthropogenic source signature as calculated from this study. Results are compared with previous studies as stated in the legend, and the shaded areas in corresponding colors show the estimated range of the sources. The arrows represent the isotopic enrichment associated with the stratospheric loss. PI = preindustrial.

Table 3
Isotopic Signature of Tropospheric N_2O in the PI Atmosphere, and Change Between the PI and Modern Periods Derived in This Study Compared to Previous Studies on Firn Air (Park et al., 2012; Röckmann, Kaiser, & Brenninkmeijer, 2003) and Combined Firn and Ice Core Air (Bernard et al., 2006; Sowers et al., 2002)

	This study[a]	Bernard et al. (2006)[a]	Sowers et al. (2002)[a]	Park et al. (2012)[a,b]	Röckmann, Kaiser, & Brenninkmeijer (2003)[a,b]
PI					
$\delta^{15}N$(‰)	9.5 ± 0.1	9.6 ± 0.1	10.1 ± 0.6	9.3 ± 0.2	8.8 ± 0.1
$\delta^{18}O$(‰)	47.1 ± 0.2	46.2 ± 0.6	47.4 ± 1.0	45.5 ± 0.2	45.8 ± 0.3
$\delta^{15}N^{\alpha}$(‰)	17.8 ± 0.4	19.0 ± 1.1	N/A	18.8 ± 1.0	19.0 ± 0.6
$\delta^{15}N^{\beta}$(‰)	1.2 ± 0.5	−0.1 ± 0.7	N/A	−0.6 ± 1.1	0.4 ± 0.6
SP (‰)	16.6 ± 0.6	18.7 ± 1.3	N/A	19.4 ± 1.5	19.4 ± 0.8
PI to modern					
$\delta^{15}N$ (‰)	2.7 ± 0.2	$2.8^{+1.0}_{-0.6}$	3.3 ± 0.8	2.5 ± 0.6	2.0 ± 0.2
$\delta^{18}O$ (‰)	2.5 ± 0.4	$1.6^{+0.3}_{-0.9}$	2.8 ± 1.3	0.9 ± 0.9	$1.2^{+0.2}_{-0.3}$
$\delta^{15}N^{\alpha}$ (‰)	2.0 ± 0.7	$3.2^{+1.0}_{-0.8}$	N/A	3.0 ± 2.2	$2.2^{+0.2}_{-0.3}$
$\delta^{15}N^{\beta}$ (‰)	3.5 ± 0.8	$2.4^{+0.9}_{-1.1}$	N/A	1.7 ± 2.1	$1.8^{+0.3}_{-0.4}$
SP (‰)	−1.5 ± 0.9	$0.8^{+6.9}_{-1.7}$	N/A	1.0 ± 3.1	$0.4^{+0.3}_{-0.4}$

Note. PI = preindustrial; SP = site preference; NEEM = North Eemian Ice Drilling Programme; EUROCORE_NM = Eurocore Greenland project.
[a]PI average isotopic composition was calculated using NEEM, EUROCORE_NM, and Siple Dome data. The differences between the PI and the modern period were calculated using average tropospheric values of the last 20 years (1989–2008) of the firn air reconstruction from Prokopiou et al. (2017), $\delta^{15}N$ = (6.8 ± 0.2)‰, $\delta^{18}O$ = (44.6 ± 0.1)‰, $\delta^{15}N^{\alpha}$ = (15.8 ± 0.1)‰, and $\delta^{15}N^{\beta}$ = (−2.3 ± 0.2)‰. [b]Values from Park et al. (2012) and Röckmann, Kaiser, and Brenninkmeijer (2003) are based on model estimates constrained by twentieth century observations.

set presented here constrains the PI isotopic composition more tightly than the previous studies. This is largely due to the higher number of samples analyzed in our study, which reduces the standard error of the mean when averaging but partly also to an increased measurement precision.

Table 3 includes the results from two studies where the isotopic composition of N_2O in the PI period are extrapolated from firn air measurements (Park et al., 2012, Röckmann, Kaiser, & Brenninkmeijer, 2003). When this approach is taken, the isotopic composition in the PI period is apparently underestimated, slightly for $\delta^{15}N^{av}$ but in a more pronounced way for $\delta^{18}O$, where the extrapolated difference between the present and PI values is only half of the measured one. This shows that simple extrapolation from the firn air measurements to the PI period is problematic, which indicates that the parameters used for the extrapolation may not have been constant in time. This will be investigated in more detail in section 4.2.

Figure 1 shows no significant variations for $\delta^{15}N^{av}$ and $\delta^{18}O$ of N_2O during the PI period. There are a few outliers for $\delta^{18}O$ that prevent detection of possible small systematic changes. For the ^{15}N isotopomers, the data set indicates potential small contrasting variations in $\delta^{15}N^{\alpha}$ and $\delta^{15}N^{\beta}$ before 500 CE and in the period between 1500 and 1700 CE. Given the analytical precision of our measurements these variations are not statistically significant, but we will qualitatively investigate processes that could cause such deviations below. The agreement between NEEM and Siple Dome measurements provides evidence that this could be a real atmospheric signal, but it should also be noted that (if $\delta^{15}N^{av}$ remains constant) $\delta^{15}N^{\alpha}$ and $\delta^{15}N^{\beta}$ by definition show opposite variations, because $\delta^{15}N^{\beta}$ is calculated from $\delta^{15}N^{av}$ and $\delta^{15}N^{\alpha}$.

4.2. Changes in the Isotopic Composition of N_2O Over the Industrial Period

In order to investigate possible changes in the isotopic composition of N_2O during the industrial period, we combined the ice core data with firn air results from a recent multisite reconstruction (Prokopiou et al., 2017). The firn study used data from six different locations, from both hemispheres to reconstruct the atmospheric history since 1940. Combining firn and ice data results extends our mole fraction and isotopic composition record to 2008 and results in a continuous isotope history from the PI period to present. A close-up view of the results for the industrial period after 1750 is provided in Figure 3.

The mole fraction records for the firn and ice measurements overlap very well, and the mole fraction continues to increase after 1940 to (322 ± 1) nmol/mol in 2008 (Figure 3a).

4.2.1. $\delta^{15}N^{av}$ and $\delta^{18}O$

All isotope signatures $\delta^{15}N^{av}$, $\delta^{18}O$, $\delta^{15}N^{\alpha}$, and $\delta^{15}N^{\beta}$ decreased from the PI to the modern period (Figures 3b–3e). The total decrease of $\delta^{15}N^{av}$ and $\delta^{18}O$ are similar, $\delta^{15}N^{av}_{PI\text{-}mod} = (2.7 \pm 0.2)‰$ and $\delta^{18}O_{PI\text{-}mod} = (2.5 \pm 0.4)‰$. In contrast, the respective changes over the LI period, from 1940 determined from the firn air samples (Prokopiou et al., 2017), are clearly different: $\delta^{15}N^{av}$decreased by (2.1 ± 0.2)‰ between 1940 and 2008, whereas $\delta^{18}O$ decreased only by (0.9 ± 0.4)‰. This indicates that $\delta^{18}O$ must have decreased much more strongly than $\delta^{15}N^{av}$ over the 1750–1940 period, to achieve a comparable total change between PI times and the modern period. The difference between the signatures is too large to be caused by the corrections for firn fractionation (see above).

Figures 4a and 4b present the firn and ice core $\delta^{15}N^{av}$ and $\delta^{18}O$ data as a function of the inverse N_2O mole fraction in order to check whether the isotope data from firn and ice core data can be explained by a single source with constant isotopic composition. If that is the case, all the data will appear along a linear regression line in the plot, which originates at the isotopic composition and mole fraction of N_2O in the PI period. We note that this is not a traditional Keeling plot which is strictly applicable only for a system without a removal term. In fact, the removal of N_2O has a significant influence on the slope and intercept of such a plot, which precludes the conventional application of obtaining an isotopic source signature. However, in Appendix A we verify that in the present situation, despite the sink term, assuming realistic source and sink strengths of N_2O, the Keeling plot approach can still be used to linearly extrapolate backward to the starting (i.e., PI) isotopic composition, which is our purpose. Errors introduced by the sink term are below 0.1‰.

Given the relatively large analytical error for the ice core measurements, no meaningful trends can be fitted to only the ice data. The firn air reconstructions, however, are much more tightly constrained (Figure 4). A feature that becomes apparent from these Keeling plots is the deviation from a linear trend for the oldest firn air data. This is related to the fact that the firn air reconstruction yields almost linear temporal trends for the isotope signatures, whereas the mole fraction increases quasi-exponentially as discussed by Prokopiou et al.

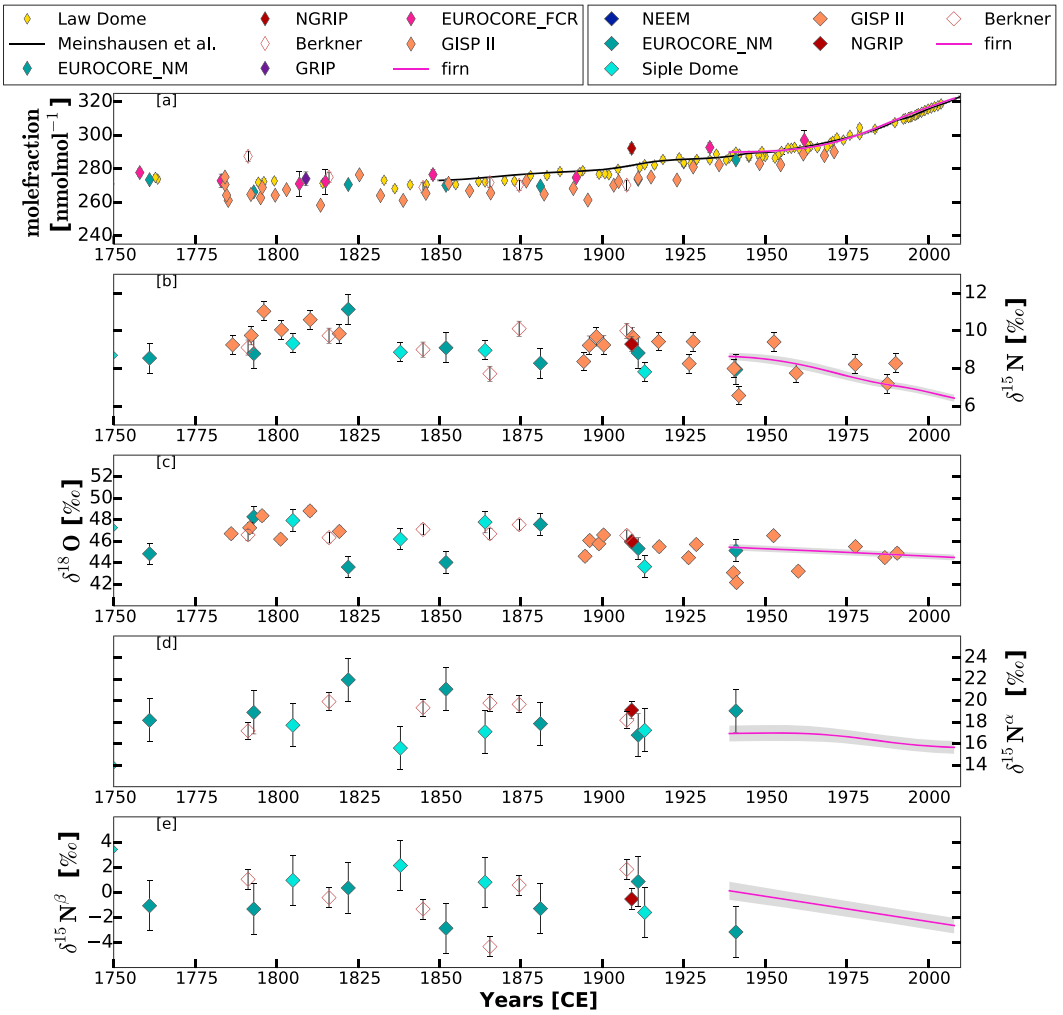

Figure 3. EUROCORE_NM and Siple Dome N_2O ice core and firn data (mole fraction and isotopic composition) covering the industrial period. (a) N_2O mole fraction from EUROCORE_NM (green diamonds), Law Dome (yellow diamonds; MacFarling Meure, 2006), Berkner Island (white diamonds; Bernard et al., 2006), and a combination of ice and firn studies (black line; Meinshausen et al., 2017), GISP II (orange diamonds; Sowers et al., 2002), GRIP (purple diamonds), EUROCORE_FCR (pink diamonds; Flückiger et al., 2002), and NGRIP (red diamonds; Bernard et al., 2006). The firn data from Prokopiou et al. (2017) are shown as magenta line. (b)–(e) $\delta^{15}N^{av}$, $\delta^{18}O$, $\delta^{15}N^{\alpha}$, and $\delta^{15}N^{\beta}$ in per mille. The color coding is the same as for mole fraction; cyan diamonds show data from Siple Dome (Rosen, 2014). The firn data from Prokopiou et al. (2017) are shown as magenta line. NEEM = North Eemian Ice Drilling Programme; EUROCORE_NM = Eurocore Greenland project; GISP = Greenland Ice Sheet Project; NGRIP = North Greenland Ice Core Project.

(2017). When these data are used to reconstruct source signatures, extremely depleted sources are required during the early part of the firn record to close the isotope budget. However, Prokopiou et al. (2017) also showed that there are isotope trajectories within the error bounds of the firn air reconstruction that do not require such depleted emissions. These scenarios result in straight lines in the Keeling plot. Hence, the very depleted source signatures that cause the curvature in the Keeling plot are not significant and are possibly due to a bias in the firn air reconstruction. Therefore, we do not use the earliest firn air data and apply a linear fit to the firn air reconstruction after year 1970. In the case of $\delta^{15}N^{av}$, this fit line intersects with the average of the ice core samples (Figure 4), which indicates that the two data sets can be used together in the nonconventional application of the Keeling plot (Appendix A). As a result it shows that for $\delta^{15}N^{av}$ the increase in N_2O since PI times can be approximated by one single representative source with a constant isotopic composition (within the experimental uncertainty). In addition, the agreement also indicates that for $\delta^{15}N^{av}$ there is no conceptual inconsistency between the independent isotope reconstructions from firn air and ice core air, respectively.

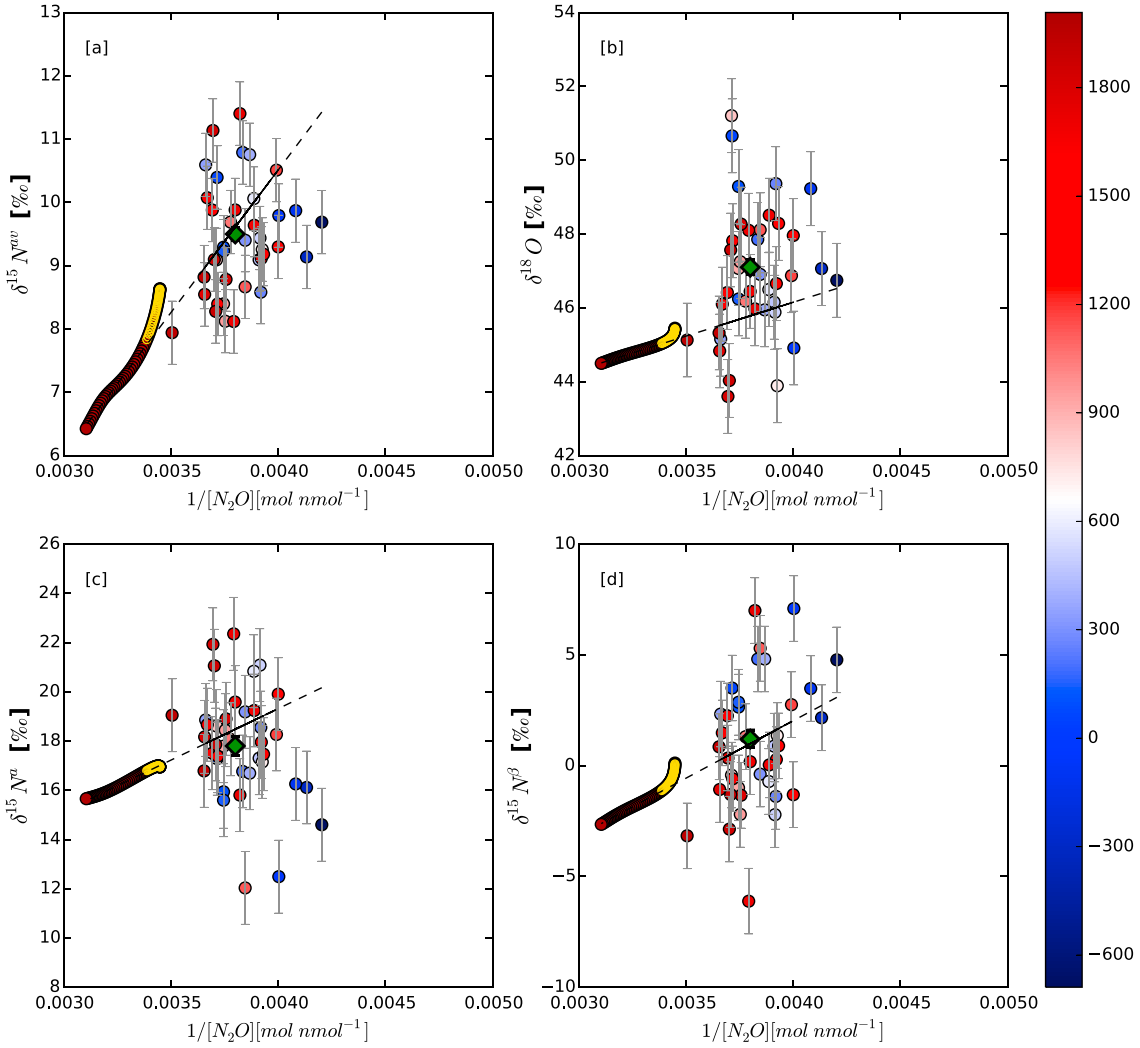

Figure 4. Keeling plot for (a) $\delta^{15}N^{av}$, (b) $\delta^{18}O$, (c) $\delta^{15}N^{\alpha}$, and (d) $\delta^{15}N^{\beta}$. For the ice samples and firn air samples after 1970, coloring indicates the age of the sample with dark blue being the oldest and dark red the youngest. Uncertainty bars indicate the standard deviation of the ice measurements. Firn air samples younger than 1970 were used for linear regression. Yellow open circles represent the firn samples before 1970. The green diamond denotes the total average of the ice data (NEEM and EUROCORE_NM), and its uncertainty is the standard error of the mean. NEEM = North Eemian Ice Drilling Programme; EUROCORE_NM = Eurocore Greenland project.

However, the same does not hold for $\delta^{18}O$. Here the extrapolation of the Keeling plot regression to the firn air data after 1970 does not intersect with the average isotopic composition of PI N_2O derived from the ice core measurements as shown in Figure 4. Apparently, in this case the modified Keeling plot model, that is, assuming one source with constant isotopic composition to be responsible for the observed increase in concentration, is not applicable. The combination of high-precision ice core data for the PI period and a well-constrained firn air history over the 1940–2008 period (Prokopiou et al., 2017) thus presents a picture of an apparent decoupling of $\delta^{15}N^{av}$ and $\delta^{18}O$ from the PI to the industrial period. This strongly supports the conclusion that Sowers et al. (2002) suggested based on a much smaller data set. The decoupling also resolves the apparent discrepancies between extrapolations from firn air data and ice core measurements in the past (Table 3; Bernard et al., 2006), because it means that the trend derived from firn air measurements cannot be simply extrapolated back to the PI atmosphere. As mentioned above for the apparent decoupling of $\delta^{15}N^{av}$ and $\delta^{18}O$, the difference in the PI isotopic composition determined from the firn and ice core data is larger than the uncertainty in the firn air correction.

4.2.2. $\delta^{15}N^{\alpha}$ and $\delta^{15}N^{\beta}$

Next, we analyze the consistency between the changes in $\delta^{15}N^{\alpha}$ and $\delta^{15}N^{\beta}$ derived from firn and ice core data. As shown in Table 3, both signatures show an overall decrease since PI times, but the decrease for

$\delta^{15}N^{\alpha}$ is (−2.0 ± 0.7)‰, whereas the decrease $\delta^{15}N^{\beta}$ is about twice as large, (−3.5 ± 0.7)‰. These results suggest that the site preference (SP) of tropospheric N_2O increased since PI times by (1.5 ± 0.9)‰. The large uncertainties in $\delta^{15}N^{\alpha}$ and $\delta^{15}N^{\beta}$ of the previous ice core measurements prevented strong quantitative constraints on the trend in SP, but in our data set the trend is statistically significant (Table 3). The change in $\delta^{15}N^{\alpha}$ since PI times agrees within combined error bars with previously published studies, and the same is true for $\delta^{15}N^{\beta}$, except for the firn air study of Röckmann, Kaiser, and Brenninkmeijer (2003), who showed significantly smaller change in the PI period from extrapolation of their firn air data.

Results from Keeling plots (Figures 4c and 4d) imply general consistency between firn and ice data sets for both position-dependent ^{15}N signatures. Once more this indicates that from the nitrogen isotope perspective the increase in N_2O can be approximated reasonably well by one typical anthropogenic source with an unchanged isotopic composition through time and that there are no conceptual problems when combining the isotope histories derived from firn and ice core data.

4.3. Possible Causes for Isotopic Variability in the PI and Industrial Periods

4.3.1. Decoupling of $\delta^{15}N^{av}$ and $\delta^{18}O$ Over the Industrial Period

A decoupling of the evolution of $\delta^{15}N^{av}$ and $\delta^{18}O$ indicates a change in source composition from the PI to the industrial period. Conceptually this can be caused by either a change in the source mix (assuming constant isotopic composition for the individual source components) or changes in the isotopic composition of one or more components (assuming a constant source mix) or a combination of both. Also, it is important to realize that only processes that have clearly different effects on $\delta^{15}N_{av}$ and $\delta^{18}O$ but collectively match our observation can lead to the apparent decoupling in the temporal trends.

As an example for a temporally changing isotopic signature, Sowers et al. (2002) suggested a shift in the latitudinal distribution of biogenic soil emissions from tropical to temperate areas as a potentially important process that could lead to a shift in $\delta^{18}O$ without a corresponding shift in $\delta^{15}N^{av}$. The $\delta^{18}O$ signature of biogenic N_2O is determined to a large degree by oxygen exchange processes involving soil water (Kool et al., 2009). Due to the latitude effect of δD and $\delta^{18}O$ in precipitation, meteoric water at higher latitudes is depleted in ^{18}O compared to the tropics, so N_2O emitted from temperate soils is expected to be depleted in ^{18}O compared to N_2O from tropical soils based on the isotopic difference of the soil waters between these regions. We note that this dependence has not yet been shown experimentally, and it may be masked by multiple other processes that affect the isotopic composition of the emitted N_2O. But in principle a poleward shift in the terrestrial emissions could lead to a decrease in $\delta^{18}O$ without a simultaneous change in $\delta^{15}N^{av}$. This could have caused the larger trend in $\delta^{18}O$ compared to $\delta^{15}N^{av}$ during the EI period.

As shown in Tables 1 and 2 and discussed in section 3, the $\delta^{15}N^{av}$ and $\delta^{18}O$ source signatures of the anthropogenic source are depleted relative to the natural source. N_2O emissions from oceans and industrial sources (automobiles, industry, and coal combustion) have $\delta^{15}N^{av}$ and $\delta^{18}O$ isotopic signatures close to the tropospheric average, while N_2O emitted from soils is depleted in both heavy isotopes (Bol et al., 2003; Dore et al., 1998; Goldberg et al., 2010; Harris et al., 2015; Kim & Craig, 1993; Naqvi et al., 1998; Opdyke et al., 2009; Pérez et al., 2001; Popp et al., 2002; Snider et al., 2015; Toyoda et al., 2008; Yoshinari et al., 1997). The fact that soil-related emissions are the main isotopically depleted source category for both natural and anthropogenic sources indicates that the agricultural soil emissions are relatively more important for the anthropogenic source than the natural soil emissions are for the natural source. There are large uncertainties to the bottom-up determination of the global average source signature of N_2O from individual source types (Snider et al., 2015), but the best estimate for soil emissions is more depleted relative to the tropospheric value for $\delta^{15}N^{av}$ than for $\delta^{18}O$ (Snider et al., 2015; Tables 1 and 2). Thus, the large impact of agricultural soil emissions could in principle affect $\delta^{15}N^{av}$ more than $\delta^{18}O$. The expected larger decrease of $\delta^{15}N^{av}$ relative to $\delta^{18}O$ could have been offset by an additional depletion of $\delta^{18}O$ by a shift in the latitudinal distribution during the EI period, as argued above and in Sowers et al. (2002), but the uncertainties are too large to draw firm conclusions.

4.3.2. Temporal Variations in $\delta^{15}N^{\alpha}$ and $\delta^{15}N^{\beta}$

Unlike $\delta^{15}N^{av}$, the ^{15}N SP of N_2O is largely independent of the isotopic signature of the precursor N species, and it has been proposed to provide more information on its production process (nitrification and denitrification; Denk et al., 2017; Popp et al., 2002; Sutka et al., 2006; Toyoda et al., 2015). Sutka et al. (2006) proposed

that nitrification and denitrification could be regarded as two end-members with strongly different SP, SP_{nitrif} = (33 ± 5)‰ and $SP_{denitr.}$ = (0 ± 5)‰. Subsequent research has indicated that the interpretation may be more complicated (Lewicka-Szczebak et al., 2014; Ostrom et al., 2007; Park et al., 2011; Schmidt et al., 2004; Sutka et al., 2006; Tilsner et al., 2003; Well et al., 2006; Well et al., 2008; Well & Flessa, 2009). Both nitrification and denitrification are multistep processes and consist of several individual steps that affect the isotopic composition. For example, Lewicka-Szczebak et al. (2014) showed that the reduction of N_2O by denitrifiers causes enrichment in heavy isotopes and can also affect research. Nevertheless, Lewicka-Szczebak et al. (2014) concluded that SP values for denitrification are much more consistent across a wide range of conditions than conventional N_2O fractionation signatures. Their recommended value for $SP_{denitr.} = -5$‰ is consistent within the uncertainty bars with the estimate from Sutka et al. (2006).

Figure 2b shows that the anthropogenic source signature for $\delta^{15}N^{\alpha}$ is more enriched compared to $\delta^{15}N^{\beta}$. Soil studies support these observations reporting enrichments in $\delta^{15}N^{\alpha}$ in N_2O signatures emitted from soils (Bol et al., 2003; Pérez et al., 2001). Another study by Park et al. (2011) provided evidence of a correlation between $\delta^{15}N^{\alpha}$ and $\delta^{15}N^{\beta}$ and $\delta^{18}O$ on emissions from soils. This is not applicable in our case since our study focuses on the total average source isotopic signature rather an individual one.

Even though the two-end-member model has weaknesses and may not be as simple as initially proposed, we follow the original mass balance approaches to investigate possible shifts between nitrification and denitrification based on SP measurements (Park et al., 2012; Prokopiou et al., 2017). As described in section 3, two periods where opposite variations in $\delta^{15}N^{\alpha}$ and $\delta^{15}N^{\beta}$ may have occurred are the period before 500 CE and that between 1500 and 1700 CE.

Rosen (2014) investigated the isotope variability during the latter period with a mass balance model in a Monte Carlo approach and concluded that only a change in nitrification versus denitrification (in the simple two-end-member model) could explain the observed opposite variations for the two ^{15}N signatures. Other processes (i.e., simple isotope source-sink disequilibrium effects, changes in troposphere-stratosphere exchange or the stratospheric sink, or varying contributions from terrestrial and oceanic sources) could not explain the observed opposite changes in $\delta^{15}N^{\alpha}$ and $\delta^{15}N^{\beta}$. The opposing trends for $\delta^{15}N^{\alpha}$ and $\delta^{15}N^{\beta}$ between 1500 and 1700 (CE) occur during the Little Ice Age. It has been shown that mole fractions of CO_2 and CH_4 decreased during the same period, which was attributed to reduced respiration of the terrestrial biosphere due to cooler temperatures for CO_2 and to cooling and predominance of dry conditions in Asia for CH_4 (Bauska et al., 2015; Mitchell et al., 2013). These conditions are expected to favor nitrification over denitrification (Butterbach-Bahl et al., 2013), in qualitative agreement with the results obtained from the SP data.

The overall trend of increasing SP from the PI to the modern period (Table 3) can be interpreted in the two-end-member (nitrification-denitrification) framework as a trend toward more nitrification with time, in agreement with earlier studies. Park et al. (2012) and Prokopiou et al. (2017) assumed the SP values for nitrification and denitrification from Sutka et al. (2006) as representative end-members. Neglecting influences from other processes, we performed the same analysis and calculated that the relative contribution of nitrification from natural sources was (7 ± 2)% and nitrification today from all sources is (24 ± 11)% meaning that the relative importance of nitrification versus denitrification production if N_2O has increased by 17 (±11)% from PI times (1750 CE) to today, in agreement with previous estimates.

5. Conclusions

We have determined the N_2O mole fraction and isotopic composition of 38 ice core samples from the Northern Hemisphere and combined them with 13 from the Southern Hemisphere covering the past three millennia. During the PI period, the isotopic composition of N_2O was $\delta^{15}N^{av}$ = (9.5 ± 0.1)‰ (vs. air-N_2), $\delta^{18}O$ = (47.1 ± 0.2)‰ (vs. Vienna Standard Mean Ocean Water), $\delta^{15}N^{\alpha}$ = (17.8 ± 0.4)‰, and $\delta^{15}N^{\beta}$ = (1.2 ± 0.4)‰ with an average N_2O mole fraction of (267 ± 1) nmol/mol. There are no significant temporal variations in the isotopic composition of N_2O in the PI period. Small possible opposite variations in $\delta^{15}N^{\alpha}$ and $\delta^{15}N^{\beta}$ may have occurred before 500 CE and between 1500 and 1700 CE, but they are also not significant.

The statistically significant increase in ^{15}N SP since PI times, together with a simplified two-end-member mixing model of denitrification and nitrification, supports earlier postulations that the relative fraction of nitrification may have increased by more than 10% since PI times.

The isotopic composition of N_2O has changed toward more depleted values for all signatures since PI times. This is not only due to a source sink imbalance, but it is likely that the isotopic signature of the total source has also decreased. Thus, the anthropogenic source of N_2O is depleted in heavy isotopes compared to the natural source, which implicates the dominance of agricultural sources, as shown in previous studies.

Our data set, combined with the firn air reconstruction from Prokopiou et al. (2017), provides strong evidence for a decoupling of the temporal evolution of $\delta^{15}N^{av}$ and $\delta^{18}O$ over the industrial period, with larger changes of $\delta^{18}O$ before 1940 and larger changes in $\delta^{15}N^{av}$ after 1940, which was postulated by Sowers et al. (2002). We propose that the stronger depletion in $\delta^{15}N^{av}$ compared to $\delta^{18}O$ expected from the increase in soil sources could have been offset by an additional depletion in $\delta^{18}O$ due to a latitudinal shift in sources as first suggested by Sowers et al. (2002). Due to this decoupling, previous studies that extrapolated the PI isotopic composition of N_2O from firn air measurements predicted about a factor 2 too small changes for $\delta^{18}O$; for the $\delta^{15}N$ isotope signatures the results between firn air extrapolations and the new ice core data set generally agree much better than for $\delta^{18}O$. Due to the large variations in the isotopic composition of N_2O from different source categories, it is not possible to clearly identify which changes were responsible for the decoupling, but it is clear that such scenarios must involve processes that change $\delta^{15}N^{av}$ differently than $\delta^{18}O$.

Appendix A: Removal term on Keeling plot

In section 4.2.2 we used a Keeling plot to illustrate the decoupling of sources contributing to the evolution of N_2O and its isotopic composition since PI times, although the Keeling plot approach is not technically applicable to a system with a removal term. Here we analyze forward calculations with our mass balance model, taking into account realistic source and sink strengths and isotope effects for N_2O, to show that the N_2O removal term does not introduce a significant error when the Keeling plot is used to extrapolate back to the PI isotopic composition.

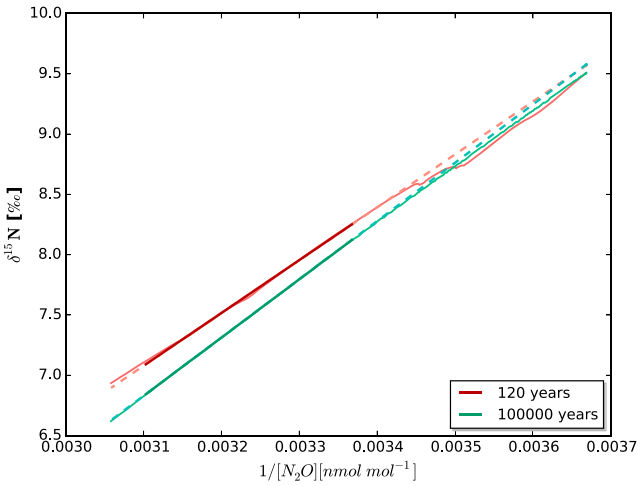

Figure A1. Results from the forward model run with constant *anthropogenic* source signature and mole fraction history constrained by Meinshausen et al. (2017) presented in a Keeling plot, similar to the analysis of the data in the main text. The model run with a 100,000-year N_2O lifetime represents basically a pure Keeling plot model with negligible sink term, while the run with 120-year lifetime is the realistic scenario (light red and light green lines for 120 and 100,000 years, respectively). The thick parts of the solid lines (dark red and dark green lines for 120 and 100,000 years, respectively) indicate the mole fraction between years 1970 and 2008 CE, the period that is used for the linear fit that is then extrapolated back to the PI mole fraction (dotted light red and green lines for 120 and 100,000 years, respectively). Although the Keeling plot itself is clearly affected by the sink term, the extrapolation back to the PI value agrees within 0.06‰ with the forward model calculations. PI = preindustrial.

In the model, the N_2O temporal evolution is taken from the high-resolution reconstruction of Meinshausen et al. (2017) who combined all published firn and ice records, to date, and constructed a continuous N_2O mole fraction history starting from year 1840 CE. The model starts with a steady state N_2O budget (for both mole fraction and isotopic composition) at year 1840 CE, the last minimum in the Meinshausen et al. (2017) reconstruction before the continuous increase. In the model we then apply an annual sink strength equivalent to a lifetime of 120 years; that is, we remove 1/120 of the atmospheric reservoir per year. The 120-year lifetime is very similar to the residence time in the atmosphere as used in the main text (123^{+29}_{-19} year). The fractionation in the sink is equal to the effective fractionation constant of the stratospheric removal as determined by Kaiser et al. (2006). After the removal step, a source of N_2O is added to fit the mole fraction history of Meinshausen et al. (2017). The fraction of the source that is needed to compensate for the sink in the PI equilibrium state is assigned the PI source signature from Table 2, and the additional fraction that causes the N_2O increase is assigned the anthropogenic signature (Table 2). This means that the isotopic composition of the total source in the model changes with time.

The results (Figure A1) show that the fractionation in the removal term changes the temporal evolution of the isotopic signature and it is not possible to use the Keeling plot in the conventional way to derive the source isotopic composition from the *y* axis intercept of the linear fit to the data. However, we do not use the Keeling plot in the traditional manner but extrapolate back from the firn air measurements (1970–2008 CE) to the PI period. We apply exactly the same approach to the time series that was created by the forward model using a constant signature for the

anthropogenic source constrained by the well-documented mole fraction evolution of Meinshausen et al. (2017) and using a realistic sink fractionation and isotopic composition of the source. Figure A1 shows that the linear extrapolation back to the PI atmosphere is still possible, and in all cases the effect of the sink is $<0.06‰$, which allows us to use the Keeling plots as done in the main text. We note that the back-extrapolated linear fit to the 100,000-year lifetime scenario shows similar offset, which reflects the changing isotopic signature of the total source (constant natural plus anthropogenic fraction).

Acknowledgments
We thank the teams involved in the ice core sampling at NEEM site during the 2008 and 2009 field seasons. NEEM is directed and organized by the Centre of Ice and Climate at the Niels Bohr Institute and U.S. NSF, Office of Polar Programs. It is supported by funding agencies and institutions in Belgium (FNRS-CFB and FWO), Canada (NRCan/GSC), China (CAS), Denmark (FIST), France (IPEV, CNRS/INSU, CEA, and ANR), Germany (AWI), Iceland (RannIs), Japan (NIPR), Korea (KOPRI), the Netherlands (NWO/ALW), and the United States (U.S. NSF, Office of Polar Programs). Acquisition of the Siple Dome Ice Core was supported by the U.S. NSF, Office of Polar Programs. Support was also provided by a U.S. NSF Graduate Research Fellowship to J. Rosen. Data will be freely available at http://www.projects.science.uu.nl/atmosphereclimate/Data.php and https://www.ncdc.noaa.gov/data-access/paleoclimatology-data/datasets/ice-core.

References

Bange, H. W., Naqvi, S. W. A., & Codispoti, L. A. (2005). The nitrogen cycle in the Arabian Sea. *Progress in Oceanography*, *65*(2-4), 145–158. https://doi.org/10.1016/j.pocean.2005.03.002

Bauska, T. K., Fortunat, J., Mix, A. C., Roth, R., Ahn, J., & Brook, E. J. (2015). Links between atmospheric carbon dioxide, the land carbon reservoir and climate over the past millennium. *Nature Geoscience*, *8*(5), 383–387. https://doi.org/10.1038/ngeo2422

Bernard, S., Röckmann, T., Kaiser, J., Barnola, J.-M., Fischer, H., Blunier, T., & Chappellaz, J. (2006). Constraints on N_2O budget changes since pre-industrial time from new firn air and ice core isotope measurements. *Atmospheric Chemistry and Physics*, (2), 493–503. 1680–7324/acp/2006–6-493. https://doi.org/10.5194/acp-6-493-2006

Bol, R., Toyoda, S., Yamulki, S., Hawkins, J. M. B., Cardenas, L. M., & Yoshida, N. (2003). Dual isotope and isotopomer ratios of N_2O emitted from a temperate grassland soil after fertilizer application. *Rapid Communications in Mass Spectrometry*, *17*(22), 2550–2556. https://doi.org/10.1002/rcm.1223, 2003.

Buizert, C., Sowers, T., & Blunier, T. (2013). Assessment of diffusive isotopic fractionation in polar firn, and application to ice core trace gas records. *Earth and Planetary Science Letters*, *361*, 110–119. https://doi.org/10.1016/j.epsl.2012.11.039

Butterbach-Bahl, K., Baggs, E. M., Dannenmann, M., Kiese, R., & Zechmeister-Boltenstern, S. (2013). Nitrous oxide emissions from soils: How well do we understand the processes and their controls? *Philosophical Transactions of the Royal Society, B: Biological Sciences*, *368*(1621), 20130122. https://doi.org/10.1098/rstb.2013.0122

Denk, T. R. A., Mohn, J., Decock, C., Lewicka-Szczebak, D., Harris, E., Butterbach-Bahl, K., et al. (2017). The nitrogen cycle: A review of isotope effects and isotope modeling approaches. *Soil Biology and Biochemistry*, *105*, 121–137. https://doi.org/10.1016/j.soilbio.2016.11.015

Denman, K., Brasseur, G., Chidthaisong, A., Ciais, P., Cox, P. M., Dickinson, R. E., et al. (2007). *Couplings between changes in the climate systems and biogeochemistry in climate change 2007: The physical science basis. Contribution of Working Group I to the Fourth Assessment Report of the Intergovernmental Panel on Climate Change*. Cambridge, United Kingdom and New York, NY, USA: Cambridge Univ. Press.

Dentener, F. J., & Crutzen, P. J. (1994). A three-dimensional model of the global ammonia cycle. *Journal of Atmospheric Chemistry*, *19*, 3342–3369.

Dore, J. E., Popp, B. N., Karl, D. M., & Sansone, F. J. (1998). A large source of atmospheric nitrous oxide from subtropical North Pacific surface waters. *Nature*, *396*(6706), 63–66. https://doi.org/10.1038/23921

Duce, R. A., LaRoche, J., Altieri, K., Arrigo, K. R., Baker, A. R., Capone, D. G., et al. (2008). Impacts of atmospheric anthropogenic nitrogen on the open ocean. *Science*, *320*(5878), 893–897. https://doi.org/10.1126/science.1150369

Environmental Protection Agency (EPA) (2010). *Methane and nitrous oxide emissions from natural sources*, EPA 430-R-10-001. Washington DC: US EPA.

Flückiger, J., Monnin, E., Stauffer, B., Schwander, J., Stocker, T., Chappellaz, J., et al. (2002). High-resolution Holocene N_2O ice core record and its relationship with CH_4 and CO_2. *Global Biogeochemical Cycles*, *16*(1), 1010. https://doi.org/10.29/2001GB001417

Forster, P., Ramaswamy, V., Artaxo, P., Berntsen, T., Betts, R., Fahey, D. W., et al. (2007). Changes in atmospheric constituents and in radiative forcing. In S. Solomon, et al. (Eds.), *Climate change 2007: The physical science basis, contribution of Working Group I to the Fourth Assessment Report of the Intergovernmental Panel on Climate Change* (Chapter 2, pp. 131–234). Cambridge, United Kingdom and New York, NY, USA: Cambridge University Press.

Goldberg, S. D., Borken, W., & Gebauer, G. (2010). N_2O emission in a Norway spruce forest due to soil frost: Concentration and isotope profiles shed a new light on an old story. *Biogeochemistry*, *97*(1), 21–30. https://doi.org/10.1007/s10533-009-9294-z

Harris, E., Zeyer, K., Kegel, R., Müller, B., Emmenegger, L., & Mohn, J. (2015). Nitrous oxide and methane emissions and nitrous oxide composition from waste incineration in Switzerland. *Waste Management*, *35*, 135–140. https://doi.org/10.1016/j.wasman.2014.10.016

Hirsch, A., Michalak, A., Bruhwiler, L., Peters, W., Dlugokencky, E., & Tans, P. (2006). Inverse modelling estimates of the global nitrous oxide surface flux from 1998–2001. *Global Biogeochemical Cycles*, *20*, GB1008. https://doi.org/10.1029/2004GB002443

Ishijima, K., Sugawara, S., Kawamura, K., Hashida, G., Morimoto, S., Murayama, S., & Aoki, S. (2007). Temporal variations of the atmospheric nitrous oxide concentration and its $\delta^{15}N$ and $\delta^{18}O$ for the latter half of the 20th century reconstructed from firn air analyses. *Journal of Geophysical Research*, *112*, D03305. https://doi.org/10.1029/2006JD007208

Ji, Q., Babbin, A. R., Jayakumar, A., Oleynik, S., & Ward, B. B. (2015). Nitrous oxide production by nitrification and denitrification in the eastern tropical South Pacific oxygen minimum zone. *Geophysical Research Letters*, *42*, 10,755–10,764. https://doi.org/10.1002/2015GL066853

Kaiser, J., Engel, A., Borchers, R., & Röckmann, T. (2006). Probing stratospheric transport and chemistry with new balloon and aircraft observations of the meridional and vertical N_2O isotope distribution. *Atmospheric Chemistry and Physics*, *6*(11), 3535–3556. https://doi.org/10.5194/acp-6-3535-2006

Kaiser, J., & Röckmann, T. (2008). Correction of mass spectrometric isotope ratio measurements for isobaric isotopologues of O_2,CO, CO_2, N_2O and SO_2. *Rapid Communications in Mass Spectrometry*, *22*(23), 3846–3850. https://doi.org/10.1002/rcm.3812

Kaiser, J., Röckmann, T., & Brenninkmeijer, C. A. M. (2003). Complete and accurate mass spectrometric isotope analysis of tropospheric nitrous oxide. *Journal of Geophysical Research*, *108*(D15), 4476. https://doi.org/10.1029/2003JD003613

Kim, K. R., & Craig, H. (1993). Nitrogen-15 and oxygen-18 characteristics of nitrous oxide: A global perspective. *Science*, *262*(5141), 1855–1857. https://doi.org/10.1126/science.262.5141.1855

Kool, D. M., Wrage, N., Oenema, O., Harris, D., & Van Groenigen, J. W. (2009). The ^{18}O signature of biogenic nitrous oxide is determined by O exchange with water. *Rapid Communications in Mass Spectrometry*, *23*(1), 104–108. https://doi.org/10.1002/rcm.3859

Kroeze, C., Mosier, A., & Bouwman, L. (1999). Closing the global N_2O budget: A retrospective analysis 1500–1994. *Global Biogeochemical Cycles*, *13*(1), 1–8. https://doi.org/10.1029/1998GB900020

Lewicka-Szczebak, D., Well, R., Köster, J. R., Fuß, R., Senbayram, M., Dittert, K., & Flessa, H. (2014). Experimental determinations of isotopic fractionation factors associated with N_2O production and reduction during denitrification in soils. *Geochimica et Cosmochimica Acta*, *134*, 55–73. https://doi.org/10.1016/j.gca.2014.03.010

Löscher, C. R., Kock, A., Könneke, M., LaRoche, J., Bange, H. W., & Schmitz, R. A. (2012). Production of oceanic nitrous oxide by ammonia-oxidizing archaea. *Biogeosciences*, *9*(7), 2419–2429. https://doi.org/10.5194/bg-9-2419-2012

MacFarling Meure, C., Etheridge, D., Trudinger, C., Steele, P., Langenfelds, R., van Ommen, T., et al. (2006). Law Dome CO_2, CH_4 and N_2O ice core records extended to 2000 years. *Journal of Geophysical Research*, *33*, L14810. https://doi.org/10.1029/2006GL026152

Meinshausen, M., Vogel, E., Nauels, A., Lorbacher, K., Meinshausen, N., Etheridge, D., et al. (2017). Historical greenhouse gas concentrations for climate modelling (CMIP6). *Geoscientific Model Development*, *10*(5), 2057–2116. https://doi.org/10.5194/gmd-10-2057-2017

Minschwaner, K., Salawitch, R. J., & McElroy, M. B. (1993). Absorption of solar radiation by O_2: Implications for O_3 and lifetimes of N_2O, $CFCl_3$, and CF_2Cl_2. *Journal of Geophysical Research*, *98*(D6), 10,543–10,561. https://doi.org/10.1029/93JD00223

Mitchell, L., Brook, E., Lee, J. E., Buizert, C., & Sowers, T. (2013). Constraints on the late Holocene anthropogenic contribution to the atmospheric methane budget. *Science*, *342*(6161), 964–966. https://doi.org/10.1126/science.1238920

Mitchell, L. E., Brook, E. J., Sowers, T., McConnell, J. R., & Taylor, K. (2011). Multidecadal variability of atmospheric methane, 1000–1800 C.E. *Journal of Geophysical Research*, *116*, G02007. https://doi.org/10.1029/2010JG001441

Naqvi, S. W. A., Yoshinari, T., Jayakumar, D. A., Altabet, M. A., Narvekar, P. V., Devol, A. H., et al. (1998). Budgetary and biogemical implications of N_2O isotope signatures in the Arabian Sea. *Nature*, *394*(6692), 462–464. https://doi.org/10.1038/28828

Opdyke, M. R., Ostrom, N. E., & Ostrom, P. H. (2009). Evidence for the predominance of denitrification as a source of N_2O in temperate agricultural soils based on isotopologue measurements. *Global Biogeochemical Cycles*, *23*, GB4018. https://doi.org/10.1029/2009GB003523

Ostrom, N. E., & Ostrom, P. H. (2011). The isotopomers of nitrous oxide: Analytical considerations and application to resolution of microbial production pathways. In M. Baskaran (Ed.), *Handbook of environmental isotope geochemisttry, advances in isotope geochemistry* (pp. 453–476). Berlin: Springer, Verlag.

Ostrom, N. E., Pitt, A., Sutka, R., Ostrom, P. H., Grandy, A. S., Huizinga, K. M., & Robertson, G. P. (2007). Isotopologue effects during N_2O reduction in soils and in pure cultures of denitrifiers. *Journal of Geophysical Research*, *112*, G02005. https://doi.org/10.1029/2006JG000287

Park, S., Croteau, P., Boering, K. A., Etheridge, D. M., Ferretti, D., Fraser, P. J., & Trudinger, C. M. (2012). Trends and seasonal cycles in the isotopic composition of nitrous oxide since 1940. *Nature Geoscience*, *5*(4), 261–265. https://doi.org/10.1038/ngeo1421

Park, S., Pérez, T., Boering, K. A., Trumbore, S. E., Gil, J., Marquina, S., & Tyler, S. C. (2011). Can N_2O stable isotopes and isotopomers be useful tools to characterize sources and microbial pathways of N_2O production and consumption in tropical soils? *Global Biogeochemical Cycles*, *25*, GB1001. https://doi.org/10.1029/2009GB003615

Pérez, T., Trumbore, S. E., Tyler, S. C., Matson, P. A., Ortiz-Monasterio, I., Rahn, T., & Griffith, D. W. T. (2001). Identifying the agricultural imprint on the global N_2O budget using stable isotopes. *Journal of Geophysical Research*, *106*(D9), 9869–9878. https://doi.org/10.1029/2000JD900809

Popp, B. N., Westley, M. B., Toyoda, S., Miwa, T., Dore, J. E., Yoshida, N., et al. (2002). Nitrogen and oxygen isotopomeric constraints on the origins and sea-to-air flux of N_2O in the oligotrophic subtropical North Pacific gyre. *Global Biogeochemical Cycles*, *16*(4), 1064. https://doi.org/10.1029/2001GB001806

Prokopiou, M., Martinerie, P., Sapart, C. J., Witrant, E., Monteil, G. A., Ishijima, K., et al. (2017). Constraining N_2O emissions since 1940 using firn air isotope measurements in both hemispheres. *Atmospheric Chemistry and Physics*, 1–50. https://doi.org/10.5194/acp-2016-487

Rahn, T., & Wahlen, M. (2000). A reassessment of the global isotopic budget of atmospheric nitrous oxide. *Global Biogeochemical Cycles*, *14*, 537–543. https://doi.org/10.1029/1999GB900070

Röckmann, T., Kaiser, J., & Brenninkmeijer, C. A. M. (2003). The isotopic fingerprint of the pre-industrial and the anthropogenic N_2O source. *Atmospheric Chemistry and Physics*, *3*(2), 315–323. https://doi.org/10.5194/acp-3-315-2003

Röckmann, T., Kaiser, J., Brenninkmeijer, C. A. M., & Brand, W. A. (2003). Gas chromatography/isotope-ratio mass spectrometry method for high-precision position-dependent ^{15}N and ^{18}O measurements of atmospheric nitrous oxide. *Rapid Communications in Mass Spectrometry*, *17*(16), 1897–1908. https://doi.org/10.1002/rcm.1132

Röckmann, T., Kaiser, J., Crowley, J. N., Brenninkmeijer, C. A. M., & Crutzen, P. J. (2001). The origin of the anomalous or "mass-independent" oxygen isotope fractionation in tropospheric N_2O. *Geophysical Research Letters*, *28*(3), 503–506. https://doi.org/10.1029/2000GL012295

Röckmann, T., & Levin, I. (2005). High-precision determination of the changing isotopic composition of atmospheric N_2O from 1990 to 2002. *Journal of Geophysical Research*, *110*, D21304. https://doi.org/10.1029/2005JD006066

Rosen, J. L. (2014). Constraints on preindustrial-modern changes in atmospheric nitrous oxide sources from position-dependent isotope measurements in ice core samples. PhD thesis, College of Earth, Ocean and Atmospheric Science, Oregon State University, Corvallis.

Santoro, A. E., Buchwald, C., Mcllvin, M. R., & Casciotti, K. L. (2011). Isotopic signature of N_2O produced by marine ammonia-oxidizing archaea. *Science*, *333*(6047), 1282–1285. https://doi.org/10.1126/science.1208239

Sapart, C. J., van der Veen, C., Vigano, I., Brass, M., van de Wal, R. S. W., Bock, M., et al. (2011). Simultaneous stable isotope analysis of methane and nitrous oxide of ice core samples. *Atmospheric Measurement Techniques*, *4*(12), 2607–2618. https://doi.org/10.5194/amt-4-2607-2011

Schilt, A., Baumgartner, M., Blunier, T., Schwander, J., Spahni, R., Fischer, H., & Stocker, T. F. (2010). Glacial-interglacial and millennial-scale variations in the atmospheric nitrous oxide concentration during the last 800,000 years. *Quaternary Science*, *29*(1-2), 182–192. https://doi.org/10.1016/j.quascirev.2009.03.011

Schilt, A., Baumgartner, M., Schwander, J., Buiron, D., Capron, E., Chappellaz, J., et al. (2010). Atmospheric nitrous oxide during the last 140,000 years. *Earth and Planetary Science*, *300*(1-2), 33–43. https://doi.org/10.1016/j.epsl.2010.09.027

Schilt, A., Brook, E. J., Bauska, T. K., Baggenstos, D., Fischer, H., Fortuanat, J., et al. (2014). Isotopic constraints on marine and terrestrial N_2O emissions during the last deglaciation. *Nature*, *516*(7530), 234–237. https://doi.org/10.1038/nature13971

Schmidt, H. -L., Werner, R. A., Yoshida, N., & Well, R. (2004). Is the isotopic composition of nitrous oxide an indicator for its origin from nitrification or denitrification? A theoretical approach from referred data and microbiological and enzyme kinetic aspects. *Rapid Communications in Mass Spectrometry*, *18*(18), 2036–2040. https://doi.org/10.1002/rcm.1586

Severinghaus, J. P., Beaudette, R., Headly, M. A., Taylor, K., & Brook, E. J. (2009). Oxygen-18 of O_2 records the impact of abrupt climate change on the terrestrial biosphere. *Science*, *324*(5933), 1431–1434. https://doi.org/10.1126/science.1169473

Severinghaus, J. P., Grachev, A., & Battle, M. (2001). Thermal fractionation of air in polar firn by seasonal temperature gradients. *Geochemistry, Geophysics, Geosystems*, *2*(7). https://doi.org/10.1029/2000GC000146

Snider, D. M., Venkiteswaran, J. J., Schiff, S. L., & Spoelstra, J. (2015). From the ground up: Global nitrous oxide sources are constrained by stable isotope values. *PLoS One*, *10*(3), 1–19.

Sowers, T., Alley, R. B., & Jubenville, J. (2003). Ice core records of atmospheric N_2O covering the last 106,000 years. *Science*, *301*(5635), 945–948. https://doi.org/10.1126/science.1085293

Sowers, T., Rodebaugh, A., Yoshida, N., & Toyoda, S. (2002). Extending records of the isotopic composition of atmospheric N_2O back to 1800 A.D. from air trapped in snow at the South Pole and the Greenland Ice Sheet Project II ice core. *Global Biogeochemical Cycles*, *16*(4), 1129. https://doi.org/10.1029/2002GB001911

SPARC (2013). SPARC Report on the Lifetimes of stratospheric ozone-depleting substances, their replacements, and related species. In M. Ko, P. Newman, S. Reimann, & S. Strahan (Eds.), SPARC Report No. 6, WCRP-15, Zurich, Switzerland.

Stocker, T. F., Qin, D., Plattner, G. -K., Tingor, M., Allen, S. K., Boschung, J., et al. (2013). *IPCC, 2013: Climate change 2013: The physical science basis, contribution of Working Group I to the Fifth Assessment Report of the Intergovernmental Panel on Climate Change*. Cambridge, United Kingdom and New York, NY, USA: Cambridge University Press.

Sutka, R. L., Ostrom, N. E., Ostrom, P. H., Breznak, J. A., Gandhi, H., Pitt, A. J., & Li, F. (2006). Distinguishing nitrous oxide production from nitrification and denitrification on the basis of isotopomer abundances. *Applied and Environmental Microbiology*, *72*(1), 638–644. https://doi.org/10.1128/AEM.72.1.638-644.2006

Syakila, A., & Kroeze, C. (2011). The global nitrous oxide budget revisited. *Greenhouse Gas Measurement and Management*, *1*(1), 17–26. https://doi.org/10.3763/ghgmm.2010.0007

Taylor, K. C., Alley, R. B., Meese, D. A., Spencer, M. K., Brook, E. J., Dunbar, N. W., et al. (2004). Dating the Siple Dome (Antarctica) ice core by manual and computer interpretation of annual layering. *Journal of Glaciology*, *50*(170), 453–461. https://doi.org/10.3189/172756504781829864

Thompson, R. L., Ishijima, K., Saikawa, E., Corazza, M., Karstens, U., & Patra, P. K. (2014). TransCom N_2O model inter-comparison, part II: Atmospheric inversion estimates of N_2O emissions. *Atmospheric Chemistry and Physics*, *14*, 5271–5321.

Tilsner, J., Wrage, N., Lauf, J., & Gebauer, G. (2003). Emission of gaseous nitrogen oxides from an extensively managed grassland in NE Bavaria, Germany. II. Stable isotope abundance of N_2O. *Biogeochemistry*, *63*(3), 249–267. https://doi.org/10.1023/A:1023316315550

Toyoda, S., Kuroki, N., Yoshida, N., Ishijima, K., Tohjima, Y., & Machida, T. (2013). Decadal time series of tropospheric abundance of N_2O isotopomers and isotopologues in the Northern Hemisphere obtained by the long-term observation at Hateruma Island, Japan. *Journal of Geophysical Research: Atmospheres*, *118*, 3369–3381. https://doi.org/10.1002/jgrd.50221

Toyoda, S., Yamamoto, S., Arai, S., Nara, H., Yoshida, N., Kashiwakura, K., & Akiyama, K. (2008). Isotopomeric characterization of N_2O produced, consumed, and emitted by automobiles. *Rapid Communications in Mass Spectrometry*, *22*(5), 603–612. https://doi.org/10.1002/rcm.3400

Toyoda, S., Yoshida, N., & Koba, K. (2015). Isotopocule analysis of biologically produced nitrous oxide in various environments. *Mass Spectrometry Reviews*, *36*(2), 135–160. https://doi.org/10.1002/mas.21459

Vinther, B. M., Clausen, H. B., Johnsen, S. J., Rasmussen, S. O., Andersen, K. K., Buchardt, S. L., et al. (2006). A synchronized dating of three Greenland ice cores throughout the Holocene. *Journal of Geophysical Research*, *111*, D13102. https://doi.org/10.1029/2005JD006921

Well, R., & Flessa, H. (2009). Isotopologue enrichment factors of N_2O reduction in soils. *Rapid Communications in Mass Spectrometry*, *23*(18), 2996–3002. https://doi.org/10.1002/rcm.4216

Well, R., Flessa, H., Xing, L., Xiaotang, J., & Römheld, V. (2008). Isotopologue ratios of N_2O emitted from microcosms with NH_4^+ fertilized arable soils under conditions favoring nitrification. *Soil Biology & Biochemistry*, *40*(9), 2416–2426. https://doi.org/10.1016/j.soilbio.2008.06.003

Well, R., Kurganova, I., de Gerenyu, V. L., & Flessa, H. (2006). Isotopomer signatures of soil-emitted N_2O under different moisture conditions—A microcosm study with arable loess soil. *Soil Biology and Biochemistry*, *38*(9), 2923–2933. https://doi.org/10.1016/j.soilbio.2006.05.003

Yoshida, N., & Toyoda, S. (2000). Constraining the atmospheric N_2O budget from intramolecular site preference in N_2O isotopomers. *Nature*, *405*(6784), 330–334. https://doi.org/10.1038/35012558

Yoshinari, T., Altabet, M. A., Naqvi, S. W. A., Codispoti, L., Jayakumar, A., Kuhland, M., & Devol, A. (1997). Nitrogen and oxygen isotopic composition of N_2O from suboxic waters of the eastern tropical North Pacific and the Arabian Sea—Measurement by continuous-flow isotope-ratio monitoring. *Marine Chemistry*, *56*(3-4), 253–264. https://doi.org/10.1016/S0304-4203(96)00073-4